THE ASTROPHYSICAL JOURNAL, 368:138–151, 1991 February 10

COORDINATED X-RAY ULTRAVIOLET AND OPTICAL OBSERVATIONS OF 3C 120[1]

L. MARASCHI,[2] L. CHIAPPETTI,[3] R. FALOMO,[4] B. GARILLI,[3] M. MALKAN,[5] G. TAGLIAFERRI,[6]
E. G. TANZI,[3] AND A. TREVES[2]

Received 1990 April 30; accepted 1990 August 1

ABSTRACT

The results of 14 observations with *EXOSAT* and 10 quasi-simultaneous observations with *IUE* of the Seyfert galaxy 3C 120 are reported. On few epochs, quasi-simultaneous optical spectrophotometry was also obtained, allowing us to derive the energy distribution from the optical to the X-ray band in different intensity states. The X-ray spectra are well-represented by a power-law model with constant interstellar absorption, with slopes varying between 1.00 ± 0.04 and 0.57 ± 0.05. The spectral slope is positively correlated with the soft (0.3–2 keV) X-ray intensity, but anticorrelated with the medium energy (3.5–6 keV) intensity, suggesting a pivoting of the spectrum around an energy of $\simeq 2$ keV. Variability with time scales shorter than 1 day is not observed in either band. The average amplitude of variability in the short UV wavelength range is larger than in the X-ray bands. The quasi-simultaneous UV observations exclude a strong correlation of the X-ray and UV fluxes with short lags, but some correlation is indicated between the flux in the highest frequency ultraviolet band (1320–1420 Å) and the flux in the soft X-ray bands (≤ 1 keV). Six observations at intervals of days seem to indicate that the medium X-ray emission lags the soft one. The implications of the results for models of production of the continuum are discussed.

Subject headings: galaxies: individual (3C 120) — galaxies: Seyfert — galaxies: X-rays — ultraviolet: spectra

I. INTRODUCTION

3C 120 is an important and well-studied source. Its optical identification is due to Clarke, Bolton, and Shimmins (1966). The emission-line spectrum ($z = 0.033$) allows a classification as a Seyfert 1 galaxy (Burbidge 1967). The radio emission has a bright core component, which is the closest and one of the most extensively observed superluminal radio sources, with a jet extending from the pc to the kpc scale (Walker, Benson, and Unwin 1987, and references therein). The optical continuum is highly variable, with color changes that can be accounted for by dilution of a hard continuum from starlight (Wlerick, Westerlund, and Garnier 1979; French and Miller 1980; Oke, Readhead, and Sargent 1980). The first ultraviolet spectra were obtained by Oke and Zimmermann (1979) showing a pronounced 2200 Å absorption feature. The dereddened energy distribution has a substantial ultraviolet excess which may be associated with an accretion disk. The optical continuum and emission lines are weakly polarized, probably with a substantial Galactic dust component, but the polarization angle of the continuum is variable, which indicates the presence of an intrinsic polarized component (Antonucci 1984).

The X-ray emission was studied by Schnopper *et al.* (1977), Tananbaum *et al.* (1978), Dower *et al.* (1980), Marshall, Warwick, and Pounds (1981), Piccinotti *et al.* (1982), and Rothschild *et al.* (1983). The latter authors, using *HEAO 1* data, showed that the X-ray spectrum of 3C 120 is well described by a power law with the "canonical" energy index, $\alpha_E = 0.7$, extending up to at least 50 keV. A detailed study by Halpern (1984) with the *EINSTEIN* monitor proportional counter revealed spectral variability with $\alpha_{1-10\,\mathrm{keV}}$ ranging from 0.5 to 0.8 for an increase in intensity by a factor of 2 at 5.6 keV.

Because of its brightness and variability, the source was chosen for a campaign of coordinated observations with *EXOSAT*, *IUE*, and ground-based telescopes aimed at studying the broad-band energy distribution and its variability. Here we report the results of this campaign, which provided 14 observations with *EXOSAT*, 10 *IUE* observations within few days from the X-ray ones, and a number of optical observations. A synoptic journal of observations is given in Table 1. Five of the *EXOSAT* observations, discussed in Turner and Pounds (1989), were obtained as part of a different program aimed at studying the correlation with the radio emission. They were retrieved from the archives and are included in the present analysis. Four additional *IUE* observations in the period 1983 August–1986 February, available from the archives are also included. Preliminary accounts of part of the program were given in Tanzi *et al.* (1984) and Maraschi *et al.* (1986*a*, *b*).

II. X-RAY OBSERVATIONS

a) Journal of Observations and Data Analysis

The 14 X-ray observations were performed with the *EXOSAT* observatory during the 3 yr lifetime of the satellite with time intervals of months, except for 1984 October, when the source was observed six times within 10 days.

A description of the *EXOSAT* instrumentation can be found in White and Peacock (1988). The data examined here are derived from the low-energy (LE) experiment, consisting of two X-ray imaging telescopes with microchannel detectors in the energy range 0.02–2 keV and from the medium-energy (ME) instrument, consisting of an array of eight proportional counters, of which we consider the Argon chambers, sensitive in the 1–20 keV range.

During the first observation, when both LE telescopes were operative, one was used with the 3000 Å Lexan (3Lx) filter, while four filters—3Lx, Aluminum-Parylene (Al/Par), Poly-

[1] Based on data obtained with the *EXOSAT* and *IUE* satellites.
[2] Dipartimento di Fisica, Università degli Studi, Milano, Italy.
[3] Istituto di Fisica Cosmica, CNR, Milano, Italy.
[4] Osservatorio Astronomico di Padova, Italy.
[5] University of California, Los Angeles, USA.
[6] Exosat Observatory, ESTEC, Noordwijk, The Netherlands.

TABLE 1

SYNOPTIC JOURNAL OF OBSERVATIONS

Date	*EXOSAT*	*IUE*	Optical
1983.....	(1) Aug 15–16	(A) Aug 17	Aug 15–16
		(B) Sep 25	
	(2) Nov 1	(C) Oct 31	Oct 31, Nov 4
			Dec 26
1984.....	(3) Jan 8	(D) Jan 8	
			Jan 27
		(E) Mar 29	
	(4) Sep 5	(F) Sep 5	
	(5) Oct 2		
	(6) Oct 3		
	(7) Oct 4	(G) Oct 4	
	(8) Oct 6		
	(9) Oct 10	(H) Oct 9	
	(10) Oct 12	(I) Oct 12	Oct 13
			Nov 9, 11
			Nov 20, 27, 29
			Dec 25
1985.....	(11) Feb 13		Feb 14, 15
		(J) Mar 27	
	(12) Oct 10–11	(K) Oct 13	
		(L) Nov 2	
1986.....	(13) Jan 31	(M) Jan 30	Jan 14
	(14) Feb 13	(N) Feb 13	

propylene (PPL), and Boron—were alternated on the second telescope. Subsequently one of the two detectors failed, and during the following observations three of the filters, 3Lx, Al/Par and Boron, were alternated in front of the remaining LE focal plane detector, except for observation 11, when only the 3Lx filter was used continuously.

In all cases, one-half of the ME array was pointed at the source and the other half was offset to monitor the background. The two halves were swapped once during each observation, except for observation 3. The medium-energy experiment was always used in the operating mode HER4, i.e., collecting 128 channel spectra in each detector every 10 s.

A detailed journal of the X-ray observations is given in Table 2. In columns (1) and (2) were reported respectively the observation number, used throughout the rest of the paper to identify the X-ray observations, and the date and time of the observation. Columns (3), (4), and (5) refer to the LE instrument and give, respectively, the filter, the exposure time, and the count rate for that filter. Columns (6), (7), and (8) refer to the ME instrument and indicate the on-source half of the counter array, the corresponding exposure time and the count rates in the 2–6 keV energy band, averaged over the complete observation, normalized to the whole instrument.

The analysis of the low-energy data was carried out with the procedure described in Giommi *et al.* (1987). In particular, nonuniformities in the detector were taken into account rescaling the measured background to the source position. Vignetting and dead time corrections were also applied. For the Boron filter, a point-spread function appropriate for 3C 120 was determined, summing the images corresponding to observations 6, 7, 8, 9, and 10. This was used to correct the count rates measured in a fixed box of 40 × 40 pixels. A systematic error of 5% was combined with the statistical one for this filter.

The analysis of ME data was carried out using the following procedure. The background spectrum for each half of the experiment was estimated from its off-source period and the resulting pulse height distribution corrected for the different alignment before performing the subtraction (Giommi *et al.* 1987). Special care was used in the background evaluation and subtraction, in particular for observations 1, 3, 5, 7, 10, 11, 13, and 14, during which strong solar activity was present: by inspection of the light curves of each detector, we picked up and eliminated from our subsequent analysis all the time intervals in which solar activity affected our data in the range 1–10 keV, where signal from the source is expected. In most of the above cases, this procedure led to a fairly good background estimate, as judged from the energy distribution of the residuals, while for observations 10, 13, and 14 the residuals of the background subtraction were still unsatisfactory. In observation 14 a continuous trend in the background was noted. We therefore adopted a different procedure, using the simultaneous background as measured from the offset half instrument. A standard correction due to the different response of the two halves was applied, resulting in larger errors associated to the net spectrum. It was not possible to recover observations 10 and 13 for spectral analysis.

b) Results

In Figures 1*a*–1*d*, we present the X-ray light curves of 3C 120 as measured in two filters of the LE experiment and two channel ranges of the ME instrument. The count rates have been normalized to the mean count rate for each band. From Figure 1 it is clear that the source intensity varies significantly between different observations even in the 10 days of 1984 October when observations were closely spaced. No significant variability was instead detected within each observation, with 3 σ upper limits of 14%–60% on time scales of 5 minutes and of less than 15% on time scales of 30 minutes. The minimum two-folding time scale defined as $t_2 = \Delta t(F_{\min}/\Delta F)$ is between 4 and 7 days for the 4 X-ray bands. Due to the rather poor sampling on these time scales these values should be regarded with caution.

The correlation of fluxes measured at various epochs in the four different bands was examined using Kendall's and Spearman's statistics and with the linear regression method including errors. The results of the three tests are equivalent. Table 3 reports the correlation coefficients obtained from the regression and the chance probability associated with the Kendall index. A positive correlation is found between the bands which are closest in energy, but the correlation weakens steadily as the difference in energy ranges increases. For instance, the 3Lx intensity is not significantly correlated with the ME fluxes.

Of particular interest is the frequent monitoring of 1984 October: the light curves within this period show a diplike behavior (Fig. 1). Comparing the lowest (0.3–2 keV) and highest (3.5–6 keV) energy bands, there is a suggestion that the dip occurs earlier at low energy, with the two minima shifted by few days (1984 Oct 4, Oct 10). Due to the small number of points, it is not possible to reach a more detailed conclusion.

In Figures 2*a* and 2*b* we report the hardness ratio (defined as the 3.5–6.5 keV to Lexan count rate ratio) versus the 3Lx and 3.5–6.5 keV count rates, respectively. In both cases, there is a hint of correlation for which the chance probability is few percent (see Table 3). The chance probability obtained from nonparametric tests decreases significantly excluding observations 3, 4, 5, and 14, while, for the linear correlation with errors it remains at the same level. It is important to stress that the hardness-intensity correlation is opposite in the two energy bands, i.e., the spectrum softens with increasing 3Lx intensity,

TABLE 2

JOURNAL OF X-RAY OBSERVATIONS

Observation Number	Epoch (UT)	Low Energy Filter	Low Energy Exposure (s)	Low Energy Count Rate (counts $s^{-1} \times 10^{-2}$)	Medium Energy Half	Medium Energy Exposure	Medium Energy Count Rate 2–6 keV (counts s^{-1} per full experiment)
1	1983 Aug 15–16	Lexan	33921	3.6 ± 0.2	h1	28770	
	09:06–07:25	Lexan[a]	18060	3.8 ± 0.2	h2	16710	
		Al/Par[a]	12536	2.8 ± 0.2	ME		4.58 ± 0.04
		Boron[a]	13456	1.4 ± 0.1			
		PPL[a]	12498	4.1 ± 0.2			
2	1983 Nov 1	Lexan	6256	4.2 ± 0.3	h1	13880	
	06:30–14:31	Al/Par	7230	3.1 ± 0.3	h2	8720	
					ME		4.41 ± 0.06
3	1984 Jan 8	Lexan	2319	4.1 ± 0.5	h2	3780	
	02:05–04:37	Al/Par	1893	3.4 ± 0.5	ME		6.18 ± 0.12
4	1984 Sept 5	Lexan	3645	3.9 ± 0.4	h1	15520	
	11:27–20:06	Al/Par	3509	3.4 ± 0.4	h2	14390	
		Boron	13956	1.7 ± 0.3	ME		6.08 ± 0.05
5	1984 Oct 2	Lexan	9368	3.9 ± 0.3	h1	26030	
	06:12–15:24	Al/Par	4027	3.4 ± 0.4	h2	11970	
		Boron	20266	1.7 ± 0.3	ME		6.51 ± 0.05
6	1984 Oct 3	Lexan	8930	3.4 ± 0.3	h1	12050	
	09:53–16:33	Al/Par	4509	3.0 ± 0.3	h2	10120	
		Boron	4577	1.4 ± 0.4	ME		5.52 ± 0.06
7	1984 Oct 4	Lexan	3522	2.8 ± 0.3	h1	12230	
	12:39–19:16	Al/Par	5629	2.7 ± 0.3	h2	6510	
		Boron	10152	1.7 ± 0.3	ME		5.93 ± 0.07
8	1984 Oct 6	Lexan	12807	3.1 ± 0.2	h1	16790	
	13:34–21:21	Al/Par	4332	2.4 ± 0.3	h2	10320	
		Boron	5937	1.1 ± 0.3	ME		5.05 ± 0.05
9	1984 Oct 10	Lexan	7698	3.5 ± 0.3	h1	9130	
	03:05–09:36	Al/Par	4619	2.6 ± 0.3	h2	11890	
		Boron	4502	1.3 ± 0.4	ME		4.80 ± 0.05
10	1984 Oct 12	Lexan	5163	3.9 ± 0.4	h1	8830	
	01:10–07:08	Al/Par	3721	2.4 ± 0.3	h2	4800	
		Boron	4945	1.5 ± 0.4	ME		6.79 ± 0.10
11	1985 Feb 13	Lexan	17975	3.6 ± 0.2	h1	4800	
	23:13–05:45				h2	6350	
					ME		4.39 ± 0.07
12	1985 Oct 10–11	Lexan	12320	3.5 ± 0.2	h1	1530	
	19:33–10:31	Al/Par	3158	2.1 ± 0.3	h2	19850	
		Boron	8807	1.8 ± 0.4	ME		4.89 ± 0.09
13	1986 Jan 31	Lexan	7313	2.0 ± 0.2	h1	4680	
	06:43–14:05	Al/Par	2244	1.8 ± 0.4	h2	3780	
		Boron	9100	0.7 ± 0.2	ME		3.94 ± 0.10
14	1986 Feb 13	Lexan	6583	2.2 ± 0.3	h1	11550	
	14:45–21:39	Al/Par	2994	1.8 ± 0.3	h2	11330	
		Boron	8776	0.8 ± 0.2	ME		3.53 ± 0.10

[a] Observation performed with LE Telescope 2.

but hardness with increasing ME intensity. This suggests that the spectrum pivots around an energy intermediate between the ranges of the two instruments.

A single power law with low energy absorption (cross sections of Morrison and McCammon 1983) was fitted simultaneously to the LE and ME data for all the observations except 10 and 13, which were heavily affected by solar activity. A positive net signal is present up to an energy between 6 and 9 keV depending on the observation [see Table 4, column (2)]. The results of the fitting procedure are reported in columns (3), (4), and (5) of Table 4 and the 90% confidence contours for the two interesting parameters α, N_H are reported in Figure 3. Although the χ^2 values indicate that the fits are acceptable, we also repeated power-law fits excluding the data from the 3Lx filter, in order to investigate the possibility of a soft excess. The results, also reported in Table 4 [columns (6), (7), (8)], confirm the slopes and N_H values of the fits to the full data, thus excluding the presence of any significant soft X-ray excess. From Figure 3 and Table 4, there is no indication of variability of the column density, whose average value $N_H = 10.8 \pm 0.8 \times 10^{20}$ cm^{-2} agrees well with the accurate measurement of the columnar hydrogen in our galaxy in the direction of 3C 120, $N_H = 12.32 \times 10^{20}$ cm^2, reported by Elvis, Lockman, and Wilkes (1989).

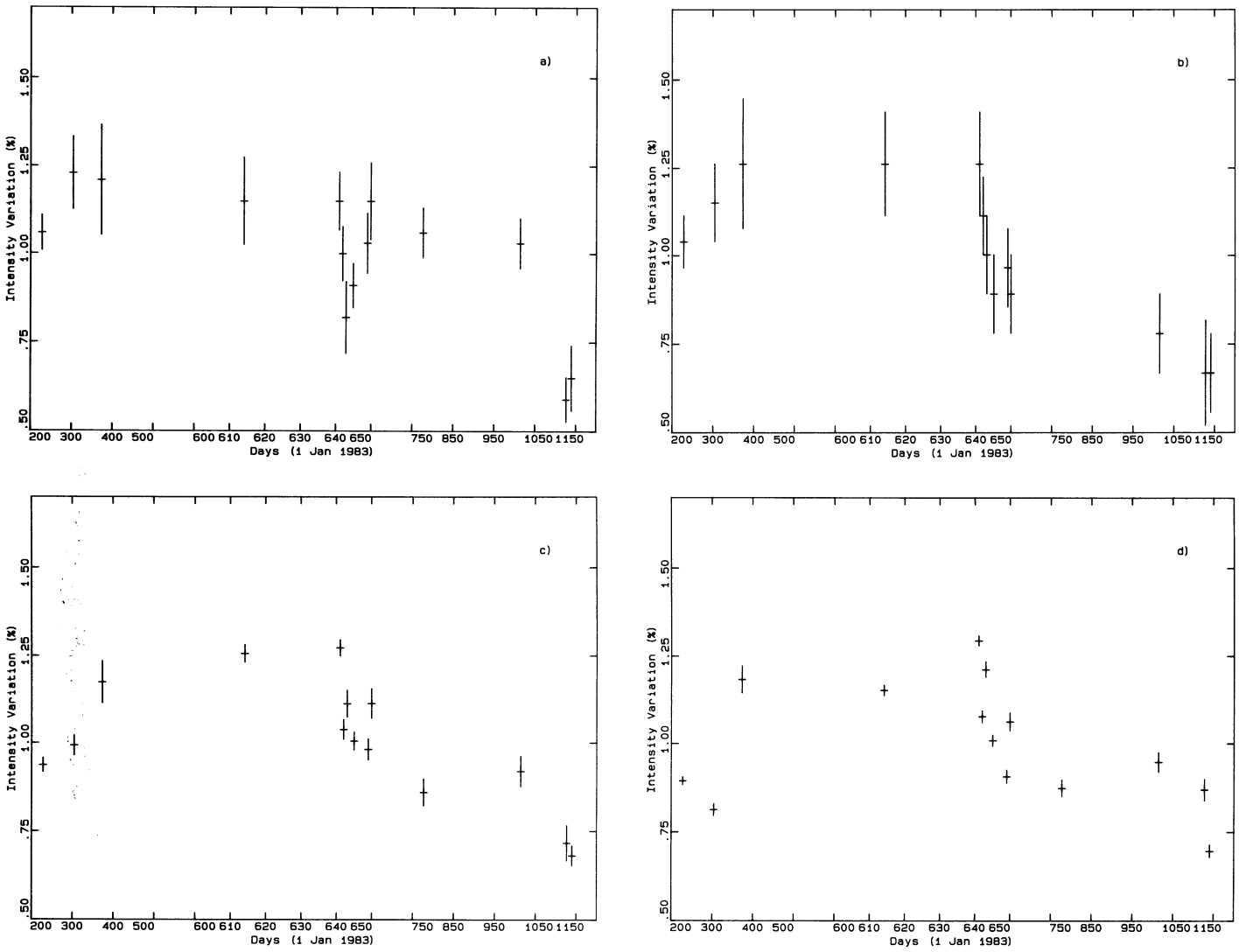

FIG. 1.—Light curves of 3C 120 in different energy bands in the period 1983 August–1986 February. For each band the intensity is normalized to the mean obtained from all the observations. The scale of times is in days after 1983 January 1. It is expanded by a factor of 10 between days 600 and 650 because of the frequent sampling in this period. (*a*) Count rate in the 3Lx filter; (*b*) count rate in the Al/Par filter; (*c*) count rate in the 1–3.5 keV band; (*d*) count rate in the 3.5–6 keV band.

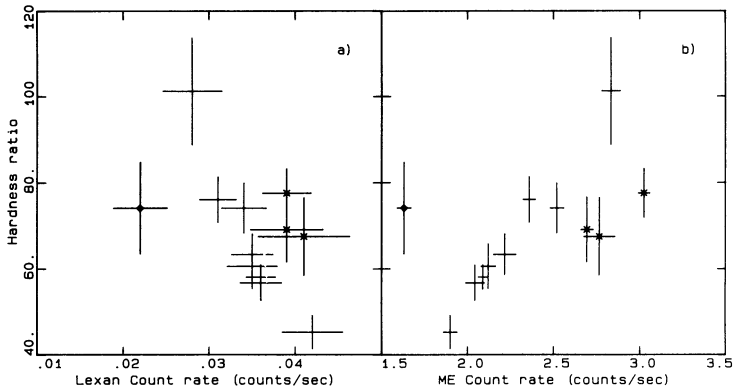

FIG. 2.—Hardness ratio, defined as the ratio of the count rate in the upper ME channels (3.5–6 keV) to the Lexan count rate, is shown as a function of the two count rates (*panel a:* Lexan count rate; *panel b:* ME count rate). Observation 14 is marked with a diamond and observations 3, 4, and 5 with asterisks (*).

TABLE 3

LINEAR CORRELATION COEFFICIENT AND KENDALL CHANCE PROBABILITY[a]

FLUX-FLUX CORRELATIONS

Linear Correlation Coefficient/ Kendall Chance Probability	UV1400	3Lx	Al/P	ME(1–3)	ME(3–6)
UV1800	0.63 5×10^{-2}	0.1 4.2×10^{-1}	0.12 7.8×10^{-1}	0.08 9.3×10^{-1}	0.18 3.2×10^{-1}
UV1400		0.4 2.2×10^{-2}	0.52 1.6×10^{-2}	0.26 8.9×10^{-2}	0.04 5.3×10^{-1}
3Lx			0.77 5.2×10^{-3}	0.72 7.2×10^{-2}	0.43 4.3×10^{-1}
Al/P				0.811 2.5×10^{-3}	0.621 2.7×10^{-2}
ME(1–3 keV)					0.87 2.4×10^{-4}

HARDNESS RATIO OR SPECTRAL INDEX-FLUX CORRELATIONS

Linear Correlation Coefficient/ Kendall Chance Probability	3Lx	ME (3–6 keV)
ME (3–6 keV)/3Lx (all observations)	0.61 4×10^{-2}	0.72 2×10^{-2}
(excluding observations 3, 4, 5, 14)	0.82 8×10^{-4}	0.96 1×10^{-3}
alpha x (all observations)	0.71 5×10^{-2}	0.53 2×10^{-1}
(excluding observations 3, 4, 5, 14)	0.89 3×10^{-2}	0.82 2×10^{-2}

[a] See text for definitions.

TABLE 4

RESULTS OF X-RAY SPECTRAL FITTING

Observation Number	Upper Energy Bound	LE + ME			LE(No Lexan) + ME			Fixed N_H		
		α (photon)	$N_H(10^{21})$ (atoms cm^{-2})	χ^2_{red} d.o.f.	α (photon)	$N_H(10^{21})$ (atoms cm^{-2})	χ^2_{red} d.o.f.	α (photon)	χ^2_{red} d.o.f.	Flux (2–6 keV)[a] (10^{-11} ergs cm^{-2} s^{-1})
1	8.0	1.70 +0.04; −0.04	0.95 +0.2; −0.2	0.74 25	1.70 +0.05; −0.05	0.86 +0.3; −0.2	0.79 24	1.75 +0.03; −0.03	1.03 26	2.5 ±0.05
2	6.9	1.94 +0.08; −0.06	1.00 +0.2; −0.2	1.20 20	1.95 +0.09; −0.07	1.0 +0.5; −0.3	1.31 19	2.00 +0.04; −0.04	1.35 21	2.4 ±0.05
3	6.3	1.78 +0.18; −0.18	1.00 +0.6; −0.4	1.20 16	1.77 +0.15; −0.15	0.9 +0.8; −0.4	1.31 15	1.82 +0.07; −0.07	1.22 17	3.3 ±0.1
4	8.7	1.85 +0.04; −0.06	1.50 +0.4; −0.4	1.30 27	1.86 +0.04; −0.06	1.7 +0.6; −0.5	1.42 26	1.82 +0.03; −0.02	1.34 28	3.5 ±0.05
5	9.0	1.70 +0.04; −0.04	1.20 +0.2; −0.2	1.50 28	1.71 +0.05; −0.05	1.22 +0.5; −0.4	1.51 27	1.71 +0.03; −0.02	1.39 29	3.8 ±0.05
6	6.9	1.68 +0.08; −0.06	1.10 +0.3; −0.2	1.60 20	1.68 +0.06; −0.08	0.96 +0.3; −0.4	1.76 19	1.70 +0.04; −0.02	1.67 21	3.2 ±0.05
7	8.4	1.54 +0.08; −0.06	1.00 +0.3; −0.3	1.20 25	1.53 +0.07; −0.07	0.75 +0.5; −0.5	1.15 24	1.57 +0.05; −0.03	1.25 26	3.5 ±0.05
8	8.1	1.68 +0.07; −0.05	1.10 +0.3; −0.3	1.50 25.00	1.69 +0.06; −0.07	1.14 +0.6; −0.4	1.56 24	1.70 +0.04; −0.03	1.47 26	2.9 ±0.05
9	7.2	1.88 +0.08; −0.08	1.30 +0.4; −0.2	0.88 22	1.88 +0.08; −0.08	1.54 +0.8; −0.5	0.89 21	1.86 +0.04; −0.04	0.87 23	2.8 ±0.05
11	6.4	1.74 +0.12; −0.1	1.00 +0.4; −0.2	1.20 16	...[b]	...	...	1.8 +0.04; −0.06	1.20 17	2.9 ±0.05
12	7.2	1.70 +0.12; −0.12	0.80 +0.4; −0.3	1.34 20	1.75 +0.11; −0.13	1.10 +0.8; −0.4	1.32 19	1.84 +0.04; −0.06	1.44 21	2.5 ±0.1
14	6.2	1.75 +0.10; −0.10	1.40 +0.6; −0.4	0.81 20	1.75 +0.15; −0.10	1.50 +1.5; −0.4	0.89 19	1.75 +0.10; −0.10	0.76 21	2.1 ±0.1

[a] Fluxes are computed using $N_H = 1.232 \times 10^{21}$ atoms cm^{-2} and spectral index as in col (9).
[b] Only Lexan filter available.

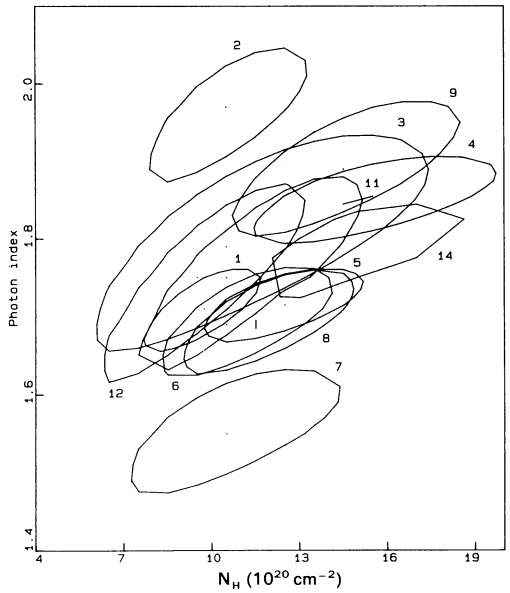

FIG. 3.—90% confidence contours for the photon spectral index and absorption column derived from power law fits for all the *EXOSAT* observations, designated here with their sequence numbers.

We therefore recomputed the spectral parameters assuming a fixed absorbing column density equal to the Galactic one, in order to diminish the uncertainty on the spectral slope. The results are reported in Table 4, columns (9) and (10). The 2–6 keV flux calculated with these spectral parameters is given in column (11). The photon index appears to vary between 2.00 ± 0.04 and $1.57^{+0.05}_{-0.03}$. The two extremes correspond to observations 2 and 7, in agreement with the fact that these observations show the smallest and largest hardness ratios as defined above. The two spectra are reported in Figures 4*a* and 4*b*. Comparing the two fits, the pivoting behavior inferred from the hardness ratios is clearly apparent, with the pivoting point located at $\simeq 2$ keV. The correlation of spectral slope with intensity gives results equivalent to those of the hardness ratio (see Table 3), but the spectral analysis shows that the variations in hardness ratio are consistent with a single power law with varying slope, rather than with changes in the column density with fixed power-law index.

A comparison of our analysis with that of Turner and Pounds (1989) concerning observations 5–11 shows that in each case the results agree within the errors, but their slopes are systematically steeper, and their absorption column is higher than ours. This effect is rather small and may derive from slightly different correction procedures applied to the LE data, which result in higher count rates in the present analysis. The absence of correlation between intensity and spectral shape reported by the above authors is not inconsistent with our results, considering that they examined a subset of all the observations.

III. ULTRAVIOLET OBSERVATIONS

a) Data Analysis

The ultraviolet observations were obtained with the *IUE* satellite. A journal of all the exposures performed in the period of the *EXOSAT* coverage is given in Table 5. The majority of the observations were taken as part of our program in near-simultaneity with the *EXOSAT* observations. Six exposures were obtained as part of a different program and were retrieved from the archives in order to increase the sampling.

The line by line spectra, generated from the raw image with the standard *IUE* spectral image processing system, were all processed with the Gaussian extraction method described by Urry and Reichert (1988) and implemented by one of us (LC) within the context of the ESO IHAP software package. This method increases the signal-to-noise ratio using a variable slit width and a local background subtraction in the extraction of the spectral intensity. The appropriate width and background

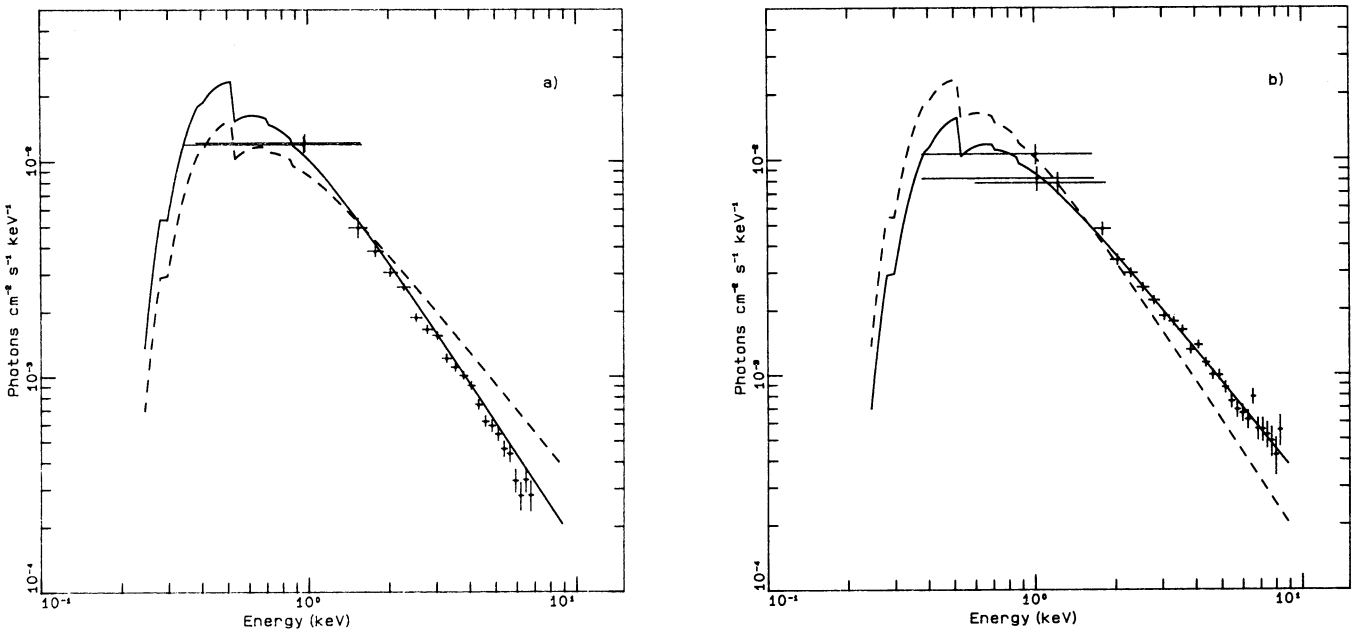

FIG. 4.—Reconstructed X-ray photon spectra are shown together with the corresponding best-fit model (*solid line*) for the steepest (observation 2, *panel a*) and flattest (observation 7, *panel b*) case, respectively. The best-fit to the other spectrum is shown for comparison as a dashed line in each panel.

TABLE 5

ULTRAVIOLET OBSERVATIONS

	Date	Image	Exposure Time (minutes)	$\langle F_\lambda \rangle$[a] (1320–1420 Å)	$\langle F_\lambda \rangle$[a] (1770–1920 Å)	$\langle F_\lambda \rangle$[a] (2500–2800 Å)
(A)	83 Aug 17	SWP 20705	270	0.69 ± 0.02	0.56 ± 0.01	
		LWR 16609	144			0.64 ± 0.01
(B)	83 Sep 25	SWP 21173	270	1.42 ± 0.02	1.08 ± 0.01	
		LWR 16874	135			0.87 ± 0.01
(C)	83 Oct 31	SWP 21419	177	1.56 ± 0.03	1.25 ± 0.01	
(D)	84 Jan 8	SWP 21969	188	1.25[b] ± 0.03	0.85 ± 0.015	
(E)	84 Mar 29	SWP 22616	270	0.875 ± 0.02	0.60 ± 0.01	
		LWP 3053	135			...[c]
(F)	84 Sep 5	SWP 23880	220	1.02 ± 0.03	0.89 ± 0.015	
		LWP 4153	130			0.81 ± 0.01
(G)	84 Oct 4	SWP 24115	210	0.83 ± 0.03	0.54 ± 0.01	
		LWP 4500	120			0.65 ± 0.01
(H)	84 Oct 9	SWP 24155	190	0.84 ± 0.03	0.59 ± 0.01	
(I)	84 Oct 12	SWP 24165	190	0.68 ± 0.03	0.73 ± 0.02	
(J)	85 Mar 27	SWP 25530	240	0.66[b] ± 0.03	0.54 ± 0.01	
		LWP 5610	135			0.59 ± 0.01
(K)	85 Oct 13	SWP 26930	90	0.64[b] ± 0.05	0.61 ± 0.01	
(L)	85 Nov 2	SWP 27009	120	0.95[b] ± 0.035	0.98 ± 0.02	
(M)	86 Jan 30	SWP 27634	110	0.62[c] ± 0.02	0.91 ± 0.02	
(N)	86 Feb 13	SWP 27709	186	0.80[b] ± 0.02	0.88 ± 0.01	

[a] F_λ in units 10^{-14} ergs s^{-1} cm^{-2} Å^{-1}.
[b] Some bad points were manually removed.
[c] Very bad S/N.

are determined by preliminarily fitting, over wide wavelength intervals, the intensity distribution perpendicular to the dispersion with a Gaussian plus a linear trend. The procedure objectively rejects regions where the signal is too weak or the background too noisy. Broad band fluxes are reported for each spectrum in Table 5.

A high-state and a low-state spectrum obtained combining exposures in the two cameras (1983 September and average of 1983 August and 1985 March, respectively) are shown in Figures 5*a* and 5*b*. Missing data correspond to camera regions rejected by the extraction procedure.

b) Continuum

The light curves for the fluxes in the two extreme bands of the short wavelength spectra, (1770–1920, 1320–1420 Å) normalized to the average value, are reported in Figures 6*a* and 6*b* on the same scale as the X-ray light curves. A large flare is present in 1983 with a two-folding time scale of 36.8 days. Other "rapid" transitions are a 30% decrease in one month between 1984 September and October and a 50% increase in 20 days in 1985 October–November.

The amplitude of the variability in the long wavelength range (Table 5), is significantly smaller than that of the corresponding short wavelength fluxes and the ratio of the fluxes in the two ranges, though available in only five cases, is well correlated with intensity, the hardness increasing with increasing intensity (Fig. 7). The same effect is not found, however, for the hardness ratio $F_{1320-1420}/F_{1770-1920}$ computed within the short wavelength range itself.

Continuum points were measured in wavelength intervals of 50 Å, in regions of sufficient signal-to-noise ratio, avoiding strong emission lines. The 1600–1750 Å region was avoided due to the possible presence of a wing of C IV and of fixed camera noise.

The continua of the two spectra shown in Figure 5 were best-fitted with a power-law distribution $F_\lambda \propto \lambda^{-\alpha_\lambda}$ reddened with the extinction curve of Seaton (1979) with variable extinction A_V. The statistical error on each point was quadratically combined with a fixed photometric error of ±5% (Hackney, Hackney, and Kondo 1984). The results are shown in Figure 5 as confidence contours for the two interesting parameters α_λ and A_V. The best-fit values of A_V are 0.85 ± 0.2 and 0.85 ± 0.4 for the high and low state, respectively, where the errors are at the 90% confidence level. We also tried blackbody fits, but these gave significantly higher χ^2 values. We therefore assumed $A_V = 0.85$ and a power-law distribution for the fits of the other spectra. The reddening value obtained is consistent with the X-ray absorption column and with the measured interstellar hydrogen column (Elvis, Lockman, and Wilkes 1989) for an average gas-to-dust ratio (e.g., Savage and Mathis 1979).

Best-fits with power laws with fixed A_V were carried out over each spectrum and, when possible, on combined spectra to cover the full 1200–3000 Å wavelength range. The results are reported in Table 6. The combined spectra show a well-defined hardening with increasing intensity (as was the case for the hardness ratios) (see Fig. 6). However, a similar effect is not present within the short wavelength range alone, which suggests that different components are present in the two ranges. In particular the contribution of the Balmer continuum and of Fe II may be large in the long wavelength range (§ V and Netzer *et al.* 1985) and the stationarity of these contributions may account for the smaller variability of the long wavelength flux and for the apparent hardening of the UV continuum.

It is remarkable that the 4 SWP spectra obtained in the last year of the program are significantly softer than all the others.

b) Lines

The lines which can be studied are Lyα, C IV, and Mg II. The profiles of the first two appear asymmetric with broader wings to the red. A detailed line study, which should refer to the entire UV data set, is beyond the scope of the present paper.

The line intensities and equivalent widths were measured

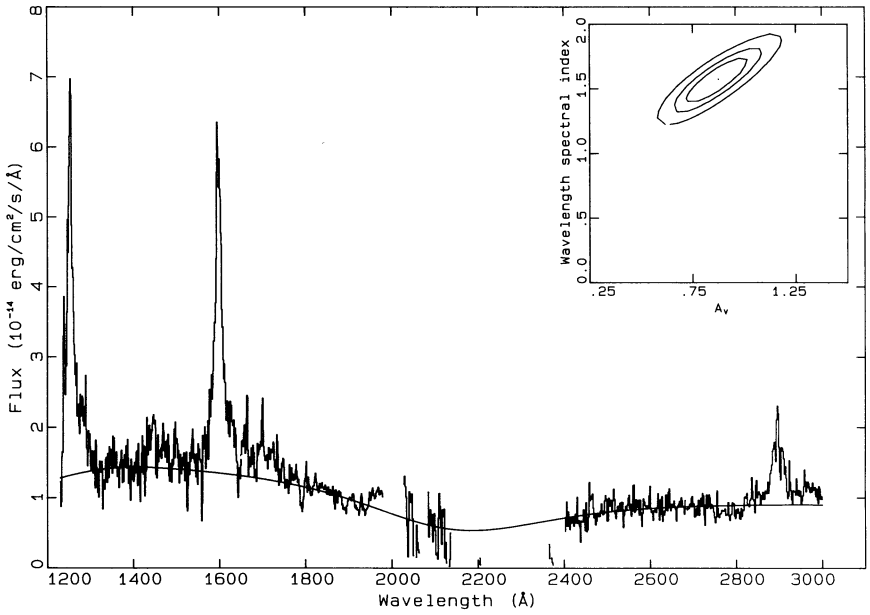

FIG. 5a

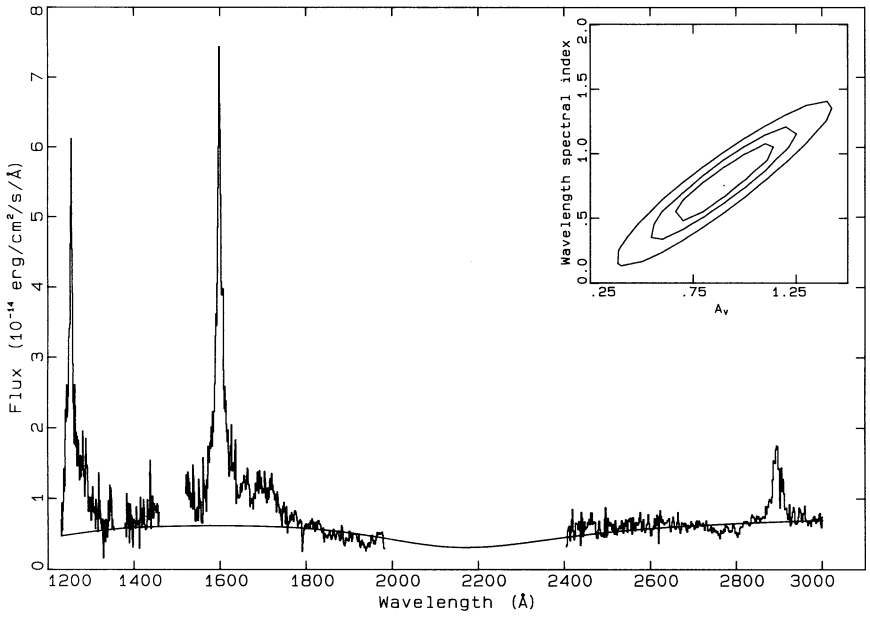

FIG. 5b

FIG. 5.—Ultraviolet spectra of 3C 120 in "high state" (observation B, *panel a*) and "low state" (average of observations A and J, *panel b*) obtained combining exposures in the two wavelength ranges of *IUE*. The best-fits obtained with a reddened power-law model are shown. Also shown, in the insets, are the 68.9% and 99% confidence contours for the fitted parameters α_λ and A_V.

with response to the best-fit continua reported in Table 6 (in the case two fits existed, one for the SWP data alone, and one for the short- and long-wavelength combination, both were used for comparison). Fixed-wavelength limits were used, which included most of the flux with the possible exception of the outermost red wing. The results are reported in Table 7. The uncertainties quoted were computed by varying the best-fit continuum values at both integration extrema, using as uncertainty the rms of the data in a corresponding 10 Å interval.

The C IV and Lyα intensities are reported in Figures 6*c* and 6*d* on the same scale as the continuum intensities. It appears that the flare in the continuum of 1983 September–October is present also in the C IV line, but with a shift in the epoch of maximum intensity of about 2 months. Our sampling is, however, too poor to set firm limits on the possible values of the suggested delay. The behavior of Lyα is unclear, possibly due to a larger observational uncertainty and or to an intrinsically smaller variability.

IV. OPTICAL AND INFRARED OBSERVATIONS

The Journal of observations, which were performed at different telescopes and by different observers, is given in Table 8.

Spectrophotometry (4000–8000 Å) was obtained at the

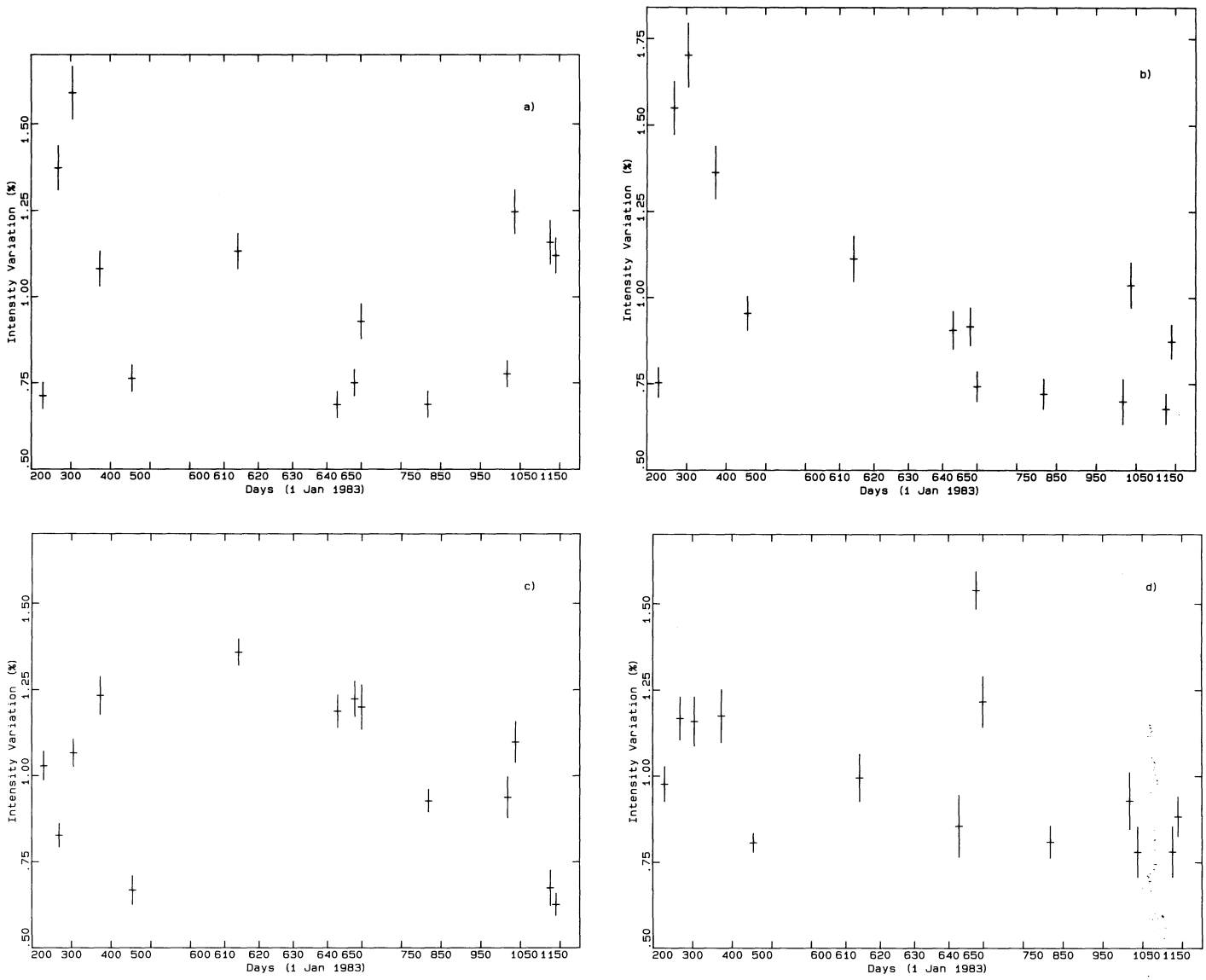

FIG. 6.—Light curves for the continuum fluxes of 3C 120 in two UV bands (1770–1920 Å and 1320–1420 Å, *panels a and b*, respectively) and for the C IV and Lyα line intensities (*panels c and d*).

European southern observatory (ESO) with an image dissector scanner (IDS) attached at the Boller and Chivens spectrograph of the ESO 1.5 and 2.2 m telescopes. An 8″ × 8″ aperture was used for each observation, but for the spectra taken on 1983 October 31 and November 4, for which the aperture was smaller. In particular, the photometric error on 1983 October 31 was larger than 10%; thus, the resulting spectrum was photometrically calibrated on the 1983 November 4 observation.

Four epochs of spectrophotometry in the range 3500–6700 Å were obtained with the photon-counting Reticon spectrograph (Hege, Cromwell, and Woolf 1979) on the Steward observatory 2.3 m telescope. The 8″ circular aperture (5″ for the 1984 January spectrum) yielded a spectral resolution of 7.5 Å (FWHM). The nights were photometric, and the agreement of several standard stars measured each night indicates the flux levels are accurate to 10%, except at the longest wavelengths, which were sometimes contaminated by second-order light. Typical integrations of 10–25 minutes produced 200–500 detected photons in each 1 Å. The spectra were reduced with C. Foltz's IRS program.

Observations were also obtained at the 1.8 m telescope of the Asiago Observatory equipped with a Boller and Chivens spectrograph with Reticon detector and with a CCD camera (Bortoletto and D'Alessandro 1986) in imaging mode.

The 1983 November observations already reported in Maraschi *et al.* (1966*a*) correspond to the UV flare. We can thus construct a quasi-simultaneous broad-band energy distribution from the optical to the X-ray band, corresponding to the brightest state in the optical and UV bands. The same can be done for 1983 August 15–17, which represents instead a low state in all bands. No other quasi-simultaneous broad-band energy distribution is available as, on 1984 October 12, solar activity heavily affected the X-ray data (see § II).

Infrared photometry was obtained at the ESO 3.6 m telescope, with the In Sb photometer, on 1983 August 15, 16, and 18, quasi-simultaneously with the first optical ultraviolet and X-ray observations. A 15″ circular aperture and a chopper

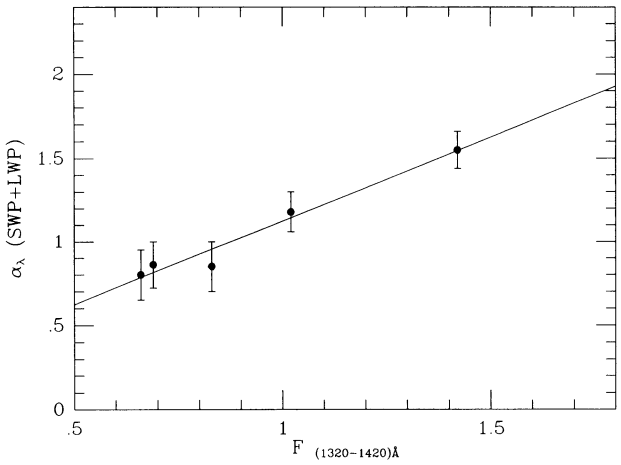

FIG. 7.—Spectral indices in the UV range derived from power-law fits with fixed reddening, $A_V = 0.85$, in the combined short + long-wavelength ranges, as a function of intensity in the 1400 Å band. The best-fit linear regression is also shown.

throw of 20″ in the east-west direction were used. The observed magnitudes are: $J = 12.58$, $H = 11.62$, $K = 10.55$, $L = 8.72$ at effective frequencies $\nu = 2.4$, 1.8, 1.4, 0.79×10^{14} Hz, respectively.

Additional observations, obtained until 1989 January in the course of an IR–optical monitoring program of AGNs, did not show any significant variability.

V. DISCUSSION

a) *Broad-Band Energy Distribution*

The broad-band energy distributions of 3C 120 derived from the quasi-simultaneous observations in 1983 August and October–November, before the onset, and near maximum of the ultraviolet flare, are shown in Figures 8*a* and 8*b*. The data have been corrected for reddening and absorption as discussed in §§ 2 and 3.

One should keep in mind that different apertures were used in different observations, which can affect the shape of the energy distribution if extended components are present. Due to the large observed variability, the X-rays and far-UV can be ascribed entirely to the nucleus, while less compact components may be present at wavelengths longer than 2000 Å. In particular, in the optical and near-IR bands, the starlight contribution is important.

The galactic intensity profile of 3C 120 was estimated from aperture photometry by Wlerick, Vesterlund, and Garnier (1979) and Moles *et al.* (1988). The *V*-magnitude of the nebulosity in a 31″ circular aperture is 15.13, according to the latter authors, which after dereddening corresponds to 7.2 mJy. What fraction of this value is appropriate for the different apertures is rather uncertain, since it depends on the models assumed in the deconvolution. We will assess this normalization from the shape of the energy distribution itself.

In both energy distributions, the ultraviolet excess which is commonly attributed to the thermal emission from an accretion disk is clearly apparent. The νf_ν representation directly shows that the bulk of the observed luminosity of 3C 120 is in this component.

Both distributions were fitted with a model of a geometrically thin, optically thick accretion disk onto a nonrotating black hole, viewed face-on. Since this is a superluminal source, it seemed reasonable to fix the inclination. All general-relativistic corrections were made, including the transfer of radiation after leaving the surface, as in Sun and Malkan (1989). Spectral regions with strong emission lines were removed from the fitting. Flux from the Balmer continuum was included, at a substantially higher level than estimated by Edelson and Malkan (1986).

Starlight was included assuming the energy distribution discussed in Malkan and Oke (1983), normalized to 3.0 mJy at 5400 Å for the 8″ × 8″ aperture (1983 August) and 2 mJy for the 4″ × 4″ aperture (1983 October). These values are consistent with our previous estimates based on the data of Wlerick, Westerlund, and Garnier (1979) (Maraschi *et al.* 1986*a*) and

TABLE 6

RESULTS OF POWER-LAW BEST-FITS TO THE UV SPECTRA

Observation	Image	α_λ[a]	Normalization[a] × 10^6	χ^2_{red}
A	SWP 20705	1.52 ± 0.3	0.35	4.72
B	SWP 21173	1.55 ± 0.3	0.87	0.47
C	SWP 21419	1.43 ± 0.3	0.40	0.33
D	SWP 21969	1.954 ± 0.3	13.25	1.09
E	SWP 22616	1.80 ± 0.3	3.35	0.31
F	SWP 23880	1.195 ± 0.3	0.048	2.83
G	SWP 24115	2.05 ± 0.35	19.2	2.03
H	SWP 24155	1.90 ± 0.3	6.5	5.61
I	SWP 24165	0.70 ± 0.4	1.0×10^{-3}	4.70
J	SWP 25530	1.58 ± 0.4	0.52	2.84
K	SWP 26930	0.34 ± 0.6	5.6×10^{-5}	7.21
L	SWP 27009	0.52 ± 0.3	3.45×10^{-4}	3.71
M	SWP 27634	−0.62 ± 0.35	5.8×10^{-8}	1.59
N	SWP 27709	0.24 ± 0.3	3.8×10^{-5}	0.83
Observation	**Image *n***	**α_λ**	**Normalization × 10^6**	**χ^2_{red}**
A	SWP 20705 + LWR 16609	0.86 ± 0.14	2.7×10^{-3}	6.45
B	SWP 21173 + LWR 16784	1.55 ± 0.11	0.86	0.83
F	SWP 23880 + LWP 4153	1.18 ± 0.12	0.04	2.17
G	SWP 24115 + LWP 4500	0.85 ± 0.15	2.4×10^{-3}	5.575
J	SWP 25530 + LWP 5610	0.80 ± 0.15	1.5×10^{-3}	3.17

[a] Normalization for $F_\lambda = k\lambda^{-\alpha\lambda}$ in units of 10^{-14} ergs cm^{-2} s^{-1} Å^{-1}, dereddened with $A_V = 0.85$.

TABLE 7

SUMMARY OF UV LINE CHARACTERISTICS

OBSERVATION	LYMAN-α[a]		C IV[b]		Mg II[c]
	SWP Fit[d]	Total Fit[e]	SWP Fit[d]	Total Fit[e]	Total Fit[e]
	Line Flux (10^{-14} ergs cm^{-2} s^{-1})				
A	79.3 ± 4.1	83.5 ± 4.6	126.3 ± 5.6	125.9 ± 5.6	29.0 ± 3.4
B	94.3 ± 5.5	95.2 ± 5.0	101.6 ± 4.7	102.5 ± 4.2	33.2 ± 4.0
C	93.5 ± 6.4	...	131.2 ± 5.2	...	...
D	95.0 ± 6.6	...	151.8 ± 7.1	...	...
E	65.2 ± 2.5	...	81.4 ± 6.1	...	...
F	80.2 ± 6.2	83.5 ± 5.4	167.1 ± 5.2	170.8 ± 5.2	35.1 ± 6.5
G	69.2 ± 7.5	81.6 ± 7.5	146.2 ± 6.1	150.9 ± 5.6	35.1 ± 1.4
H	124.3 ± 5.0	...	150.6 ± 6.6	...	...
I	98.1 ± 6.6	...	147.9 ± 8.0	...	...
J	65.7 ± 3.7	72.3 ± 4.6	113.6 ± 4.7	116.4 ± 4.7	26.0 ± 2.6
K	75.0 ± 7.1	...	114.9 ± 8.0	...	...
L	62.9 ± 6.3	...	134.7 ± 8.0	...	...
M	63.0 ± 6.4	...	82.5 ± 7.0	...	...
N	71.3 ± 5.1	...	76.5 ± 4.7	...	...
	Equivalent Width (Å)				
A	$122.0^{+28.1}_{-21.0}$	$149.8^{+43.9}_{-28.0}$	$186.8^{+46.7}_{-28.6}$	$183.7^{+45.4}_{-27.9}$	$42.3^{+9.2}_{-6.0}$
B	$71.7^{+11.8}_{-8.4}$	73.4 ± 11.1	$75.1^{+9.3}_{-6.6}$	76.8 ± 8.6	$37.1^{+8.1}_{-5.9}$
C	$65.1^{+12.9}_{-8.7}$	...	87.5 ± 10.0	...	...
D	$79.3^{+17.6}_{-12.1}$	...	$136.6^{+26.9}_{-19.6}$	...	...
E	$75.7^{+10.4}_{-6.6}$	...	$97.7^{+25.6}_{-13.6}$	...	...
F	$87.2^{+23.4}_{-14.1}$	$98.7^{+23.8}_{-17.8}$	$162.6^{+23.4}_{-15.9}$	$179.2^{+27.4}_{-18.4}$	$44.3^{+17.0}_{-11.6}$
G	$84.6^{+32.9}_{-20.7}$	$151.4^{+87.3}_{-42.0}$	$197.7^{+48.5}_{-32.7}$	$232.8^{+59.3}_{-41.7}$	$52.9^{+4.2}_{-1.6}$
H	$152.3^{+30.7}_{-17.9}$	...	$198.4^{+51.2}_{-34.1}$	...	...
I	$148.2^{+56.8}_{-30.0}$	...	$181.5^{+55.0}_{-37.2}$	...	...
J	$104.1^{+22.6}_{-17.3}$	$149.8^{+52.0}_{-25.7}$	$175.3^{+37.7}_{-20.5}$	$196.5^{+45.8}_{-27.5}$	$42.3^{+7.7}_{-5.3}$
K	$158.3^{+102.0}_{-45.2}$	...	$174.7^{+71.1}_{-37.0}$	...	...
L	$77.1^{+25.9}_{-15.6}$	...	$125.4^{+30.2}_{-18.9}$	...	...
M	$135.9^{+78.0}_{-37.5}$	...	$101.5^{+30.8}_{-18.1}$	...	...
N	$108.1^{+31.9}_{-19.1}$	...	$81.8^{+14.4}_{-8.5}$	...	...

[a] Computed in range 1230–1275 Å.
[b] Computed in range 1575–1625 Å.
[c] Computed in range 2860–2920 Å.
[d] Continuum assumed from fit to short wavelength data (Table 6, *top panel*).
[e] Continuum assumed from fit to short + long wavelength data (Table 6, *bottom panel*).

TABLE 8

OPTICAL OBSERVATIONS OF 3C 120 FROM 1983 AUGUST TO 1986 FEBRUARY

Data	Instrument	Observer[a]	$F(5500)$[b]	Note
83 Aug 15	ESO 1.5 + BC + IDS	jd	37±3	8″ × 8″
83 Aug 16	ESO 1.5 + BC + IDS	jd	38±3	8 × 8
83 Oct 31	ESO 1.5 + BC + IDS	gc	67	4 × 2
83 Nov 4	ESO 1.5 + BC + IDS	gc	55±5	4 × 4
83 Dec 26	ESO 2.2 + BC + IDS	sc	47±5	8 × 8
84 Jan 27	Steward 2.5 + RET	mm	47±3	5 × 5
84 Oct 13	Steward 2.5 + RET	mm	32±3	8 × 8
84 Nov 9	ESO 1.5 + BC + IDS	rf	30±3	8 × 8
84 Nov 11	ESO 1.5 + BC + IDS	rf	31±3	8 × 8
84 Nov 20	Steward 2.5 + RET	mm	32±3	8 × 8
84 Nov 27	ASG 1.8 + BC + RET	rf	36±4	8 × 8
84 Nov 29	ASG 1.8 + BC + RET	rf	30±3	8 × 8
85 Feb 14	Steward 2.5 + RET	mm	40±4	8 × 8
85 Feb 15	Steward 2.5 + RET	mm	38±4	8 × 8
86 Jan 14	ASG 1.8 + CCD ima	rf	43±3	V phot (15″ dia)

[a] Observers: John Danziger (jd), Guido Chincarini (gc), Stefano Cristiani (sc), Matt Malkan (mm), Renato Falomo (rf).
[b] Continuum fluxes are given in units of 0.1 mJy.

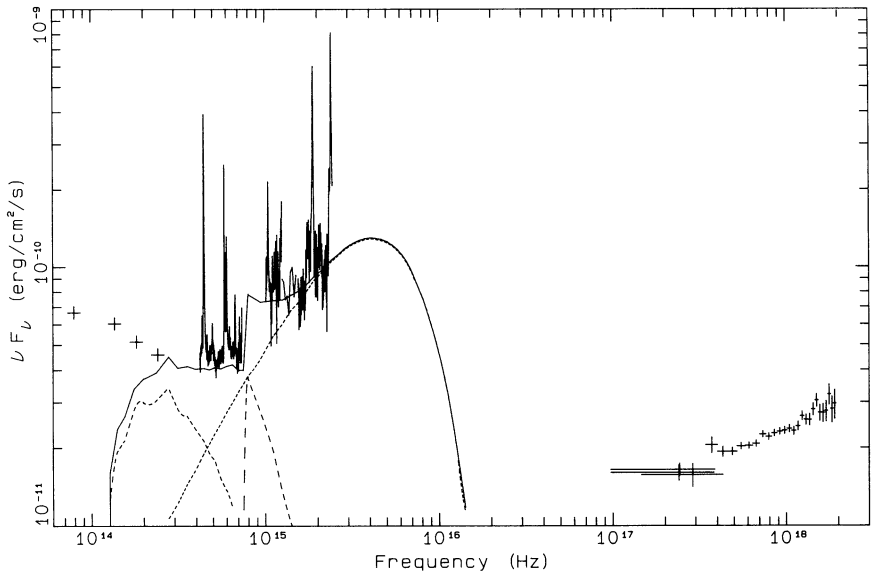

FIG. 8*a*

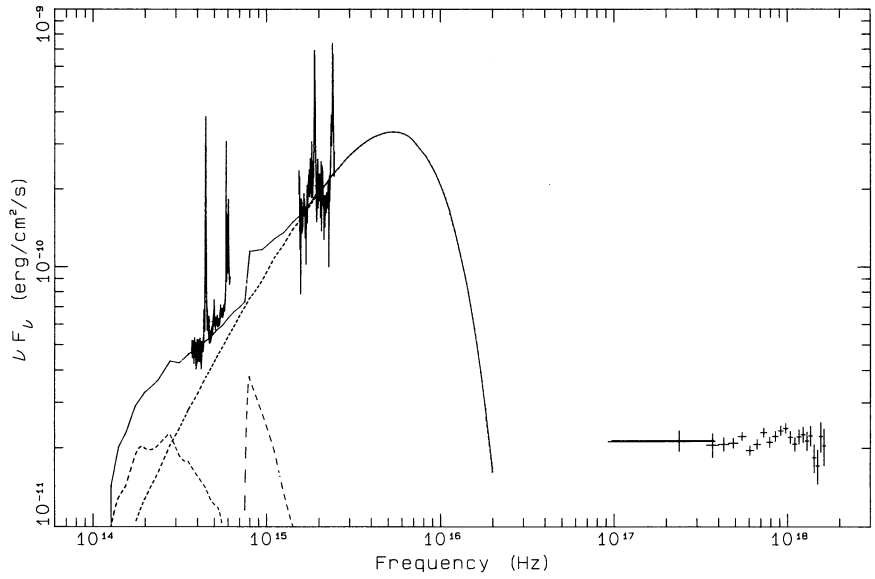

FIG. 8*b*

FIG. 8.—Composite energy distributions in vF_ν representation as from quasi-simultaneous observations on 1983 August 15 (panel a) and October 31–Nov 1 (panel b). Dashed lines represent the emission components (galactic starlight, Balmer continuum, accretion disk) adopted to fit the energy distribution. The solid line is the sum of the three components.

with the flux assumed by Edelson and Malkan (1986), but are somewhat in excess with respect to the aperture photometry of Moles *et al.* (1988).

An additional component is required to fit the IR excess apparent in Figure 8*a*. Both thermal and nonthermal explanations have been proposed for this long-wavelength emission (e.g., Edelson and Malkan 1986; Sanders *et al.* 1989), and the present analysis, which focuses on spectral bands at higher frequencies, is not apt to resolve the question. We simply note that, in the case of 3C 120, a power-law fit to the infrared data should have an energy index steeper than 1.4. Therefore, its contribution at higher frequencies would be small, and we will not discuss it further here.

Figure 8 shows that the hardening of the optical–UV continuum in the high-intensity state can be explained by two components of constant spectral shape, the galaxy and the accretion disk, which are present in different proportions at the two epochs. In the high state, the disk component is brighter and, due to the small aperture used, the galactic component is less important.

The derived accretion disk parameters are an accretion rate of 0.23 and 0.6 $M_\odot$ yr^{-1}, onto a black hole of 4×10^7 $M_\odot$, for the 1983 August and October states, respectively. Because we lack spectral coverage at wavelengths shorter than Lyman-α, these parameters are not well-constrained: adequate fits can be obtained by varying them up to 35%. In this fit, we assumed the black hole was nonrotating; as discussed in Sun and Malkan (1989), equally acceptable fits could also have been

obtained assuming a rotating (Kerr) hole with a larger mass and lower accretion rate.

The fitted disk parameters are within the range Sun and Malkan (1989) found for several other bright Seyfert 1 nuclei and low-luminosity quasars, although the luminosity is a higher fraction of the Eddington limit (18% and 47%) than the average they found. The derived mass value agrees surprisingly well with that obtained for the same object by Padovani and Rafanelli (1988) on the basis of independent arguments. However, as mentioned above, due to the lack of spectral coverage in the peak region of the disk emission, our value is only indicative, and the agreement may be coincidental.

As in the other accretion disk fits of Sun and Malkan (1989) and Band and Malkan (1989), the simple disk model assumed does not produce enough high-frequency flux to match the observed X-ray flux. However, it is expected that additional effects, especially from Comptonization and a possible optically thin central region, would substantially enhance the X-ray production, at least in the soft band, and may even extend it up to the hard X-ray band. (Czerny and Elvis 1987; Wandel and Petrosian 1988; Maraschi and Molendi 1990).

It is notable that the highest UV state corresponds to the softest X-ray spectrum.

b) X-Ray Spectral Variability

Within the X-ray band, (§ II) we find a quasi-systematic pattern of spectral variability. With few exceptions, the spectrum steepens (softens) when the low-energy intensity increases, while the opposite is true above 2–3 keV, which represents a pivoting point for the spectrum. This behavior is different from that reported by Halpern (1984), which shows softening with increasing 2–6 keV intensity, implying that a pivoting point, if present, should occur above 6 keV. Comparing the 2–10 keV fluxes, derived from our best-fits, with those given by Halpern (1984), ours appear to be 50% higher on average. Since the spectral softening reported by the above author seems to level off at high intensity, it is possible that our results represent an extension of his in a higher intensity range.

In some other Seyfert galaxies, NGC 4051, MCG-6-30-15, NGC 4151, NGC 5548, NGC 7314, and MCG-8-11-11 spectral variability has been reported (see Matsuoka *et al.* 1989; Fiore, Perola, and Romano 1990; Treves *et al.* 1990, and references therein). In all these cases the trend was toward softening with increasing intensity in the full 2–10 keV band. On the whole, the X-ray spectral behavior of 3C 120 may be thought to be analogous to that of other Seyfert galaxies, but with a somewhat lower pivoting energy. For BL Lac objects, the X-ray spectrum is observed to become harder with increasing intensity (e.g., Maraschi and Maccagni 1988; Giommi *et al.* 1989), with a possible pivoting point at ultrasoft X-ray energies. The presence of a strong superluminal radio jet in 3C 120 may be responsible for its intermediate X-ray properties.

Some correlation of the hardest UV intensity with the softest X-ray channels is indicated at a marginal confidence level. The weakness of the correlation and the fact that the variability amplitude is larger in the UV than in X-rays suggest, however, that X-ray reprocessing is not an important mechanism for the production of the UV flux, unless special conditions are involved.

If X-rays are produced by Compton scattering of the UV photons on either relativistic or hot electrons, a correlation of the two fluxes is expected in the simplest models, where the electron population is assumed fixed. However, the correlation between the observed fluxes may be lost if the electron density and/or temperature adjust to a new equilibrium value as a result of the variation of the UV photon flux (e.g., Lightman and Zdziarski 1987).

Let us discuss in more detail two models for the production of the X-ray continuum in AGNs: (*a*) Comptonization of soft photons by hot thermal electrons and (*b*) Comptonization by relativistic electrons in pair plasmas.

In the first case, the observed spectral steepening with increasing soft X-ray intensity suggests an increase in the injection rate of soft photons. A higher injection rate in a constant Comptonizing atmosphere yields higher intensity with constant spectral shape, and therefore it cannot account for the observed spectral variations. However, if, as a consequence of the increased cooling rate, the temperature of the atmosphere decreases, a softer spectrum results, and the pivoting energy should be intermediate between that of the soft photons and $3kT$. We suggest that this scheme is an interesting possibility for the case of 3C 120 and should be explored quantitatively. The model predicts that high states in the UV correspond to soft X-ray spectra, in qualitative agreement with our data.

In the pair plasma model, in which relativistic electrons scatter on an external source of soft photons, the reprocessed spectrum is predicted to steepen when the compactness parameter increases, which, for an emitting region of constant size, corresponds to an increase in luminosity (Done and Fabian 1989). Also in this model, a pivoting behavior is expected, with a pivoting energy which depends on the energy of the injected electrons and is usually very high, beyond $m_e c^2$. Thus, the behavior of 3C 120 is not consistent with this type of model.

VI. SUMMARY AND CONCLUSIONS

Our X-ray data show unambiguously that the X-ray spectrum of 3C 120 varies in slope. The spectrum softens when the X-ray intensity increases, but hardens when the medium energy X-ray intensity increases. Thus, the spectral behavior is complex and can be thought of as a pivoting around an energy of $\simeq 2$ keV.

The average, normalized variability amplitude of the far-ultraviolet flux (1200–2000 Å) is larger than that of any X-ray band. The highest frequency (1320–1420 Å) UV band shows a weak correlation with the low-frequency X-ray bands (3Lx and Al/Par filters), while no correlation is present between UV and X-ray fluxes in other bands. This refers to quasi-simultaneous observations, that is, lags shorter than 1 day. The sampling of our observations is insufficient to draw any firm conclusion on possible delayed correlations at larger lags.

The UV flux in the 2000–3000 Å range is less variable than at shorter wavelengths, which suggests the presence in this band of contributions from emission regions of intermediate size, perhaps intermediate regions of an accretion disk.

The optical–UV energy distribution can be described with an optically thick accretion disk plus starlight and Balmer continuum. The bulk of the observed luminosity is in the ultraviolet, which is consistent with the adopted disk model.

For the X-ray emission, the observations favor a model in which X-rays arise through Comptonization of soft photons produced in the innermost region of the disk by hot thermal electrons in a surrounding corona.

While the present observations are still inconclusive, they show the potential of X-ray–UV correlation studies for the understanding of the emission processes in AGNs. The limitation is not in the sensitivity of the necessary instruments, but

in the availability of sufficient time to perform these programs. It is expected that future missions, starting with the ROSAT north polar survey will allow significative advances in this direction.

We are grateful to the staff of the VILSPA station and of the *EXOSAT* observatory for their collaboration, in particular for help with scheduling and for performing some service observations. We wish to thank John Danziger, Guido Chincarini, and Stefano Cristiani for providing some optical spectra of 3C 120. B. G. wishes to thank C. Moriggio for her readiness and care in processing the original tapes. Useful comments from G. Ghisellini on the discussion section are acknowledged. We acknowledge financial support from the Ministero Università e Ricerche Scientifica and from Consiglio Nazionale delli Ricerche.

REFERENCES

Antonucci, R. J. 1984, *Ap. J.*, **278**, 499.
Band, D. L., and Malkan, M. A. 1989, *Ap. J.*, **345**, 122.
Bortoletto, F., and D'Alessandro, M. 1986, *Rev. Sci. Instr.*, **57**, 253.
Burbidge, E. M. 1967, *Ap. J. (Letters)*, **149**, L51.
Clarke, M. E., Bolton, J. G., and Shimmins, A. J. 1966, *Australian J. Phys.*, **19**, 375.
Czerny, B., and Elvis, M. 1987, *Ap. J.*, **321**, 305.
Done, C., and Fabian, A. 1989, *M.N.R.A.S.*, **240**, 81.
Dower, R. G., Griffiths, R. R., Brandt, H. V., Doxsey, R. E., and Johnston, M. D. 1980, *Ap. J.*, **235**, 355.
Edelson, R. R. A., and Malkan, M. A. 1986, *Ap. J.*, **308**, 59.
Elvis, M., Lockman, F. J., and Wilkes, B. J. 1989, *A.J.*, **97**, 777.
Fiore, F., Perola, G. C., and Romano, M. 1990, *M.N.R.A.S.*, in press.
French, H. B., and Miller, J. S. 1980, *Pub. A.S.P.*, **92**, 753.
Giommi, P., Barr, P., Garilli, B., Gioia, I. M., Maccacaro, T., Maccagni, D., and Schild, R. E. 1987, *Ap. J.*, **322**, 662.
Giommi, P., Barr, P., Garilli, B., Maccagni, D., and Pollock, A., M. T. 1989, *EXOSAT* preprint 113.
Hackney, R. L., Hackney, K. R., and Kondo, Y. 1984, *Advances in Ultraviolet Astronomy: Four Years of IUE Research*, ed. Y. Kondo, J. M. Mead, and R. D. Chapman, NASA CR 2238, p. 235.
Halpern, J. P. 1984, *Ap. J.*, **290**, 130.
Hege, H., Cromwell, C., and Woolf, W. 1979, *Adv. Electronics Electron. Phys.*, **52**, 397.
Lightman, A. P., and Zdziarski, A. A. 1987, *Ap. J.*, **319**, 643.
Malkan, M. A., and Oke, J. B. 1983, *Ap. J.*, **265**, 92.
Maraschi, L., Chiappetti, L., Danziger, J., Falomo, R., Tanzi, E. G., and Treves, A. 1986*a*, in *New Insights in Astrophysics: 8 Years of Astronomy with IUE* (ESA-SP 263), p. 613.
Maraschi, L., and Maccagni, D. 1988, *Mem. Soc. Astr. Italiana*, **59**, 277.
Maraschi, L., and Molendi, S. 1990, *Ap. J.*, **353**, 452.
Maraschi, L., *et al.* 1986*b*, in *IAU Symposium 121, Observational Evidence of Activity in Galaxies*, ed. E. Y. Khachikian, K. J. Fricke, and J. Melnick (Dordrecht: Reidel), p. 215.
Marshall, N., Warwick, R. S., and Pounds, K. A. 1981, *M.N.R.A.S.*, **194**, 987.
Matsuoka, M., Yamachi, M., Piro, L., and Murakami, T. 1989, *Ap. J.*, in press.
Moles, M., del Olmo, A., Masegosa, J., and Peres, J. D. 1988, *Astr. Ap.*, **197**, 1.
Morrison, R., and McCammon, D. 1983, *Ap. J.*, **270**, 119.
Netzer, H., Wamsteker, W., Wills, B. J., and Wills, D. 1985, *Ap. J.*, **292**, 143.
Oke, J. B., Readhead, A. C. S., and Sargent, W. L. W. 1980, *Pub. A.S.P.*, **92**, 758.
Oke, J. B., and Zimmermann, B. 1979, *Ap. J. (Letters)*, **231**, L13.
Padovani, P., and Rafanelli, P. 1988, *Astr. Ap.*, **205**, 53.
Piccinotti, G., Mushotzky, R. F., Boldt, E. A., Holt, S. S., Marshall, F. E., Serlemitsos, P. J., and Shaffer, R. A. 1982, *Ap. J.*, **253**, 485.
Rothschild, R. E., Mushotzky, R. F., Baity, W. A., Gruber, D. E., Matteson, J. L., and Peterson, L. E. 1983, *Ap. J.*, **269**, 423.
Sanders, D. B., Phinney, E. S., Neugebauer, G., Soifer, B. T., and Matthews, K. 1989, *Ap. J.*, **347**, 29.
Savage, B. D., and Mathis, J. S. 1979, *Ann. Rev. Astr. Ap.*, **17**, 73.
Schnopper, H. W., Epstein, A., Delvaille, J. P., Tucker, W., Doxsey, R., and Jermigan, G. 1977, *Ap. J. (Letters)*, **215**, L7.
Seaton, M. J. 1979, *M.N.R.A.S.*, **187**, 785.
Sun, W. H., and Malkan, M. A. 1989, *Ap. J.*, **346**, 68.
Tananbaum, H., Peters, G., Forman, W., Giacconi, R., Jones, C., and Avni, Y. 1978, *Ap. J.*, **223**, 74.
Tanzi, E. G., *et al.* 1984, in *Proc. 4th European IUE Conf.*, ed. E. Rolfe and B. Battrich (ESA-SP 218), p. 111.
Treves, A., Bonelli, G., Chiappetti, L., Falomo, R., Maraschi, L., Tagliaferri, G., and Tanzi, E. G. 1990, *Ap. J.*, in press.
Turner, T. J., and Pounds, K. A. 1989, *M.N.R.A.S.*, **240**, 833.
Urry, M., and Reichert, A. 1988, *IUE NASA Newsletter*, No. 34.
Walker, R. C., Benson, J. M., and Unwin, S. C. 1987, *Ap. J.*, **316**, 546.
Wandel, A., and Petrosian, V. 1988, *Ap. J. (Letters)*, **329**, L11.
White, N. E., and Peacock, A. 1988, *Mem. Soc. Astr. Italiana*, **59**, 7.
Wlerick, G., Westerlund, B., and Garnier, R. 1979, *Astr. Ap.*, **72**, 277.

L. CHIAPPETTI: Istituto di Fisica Cosmica, CNR Via Bassini, 15 20133 Milano, Italy

R. FALOMO: Osservatorio Astronomico di Padova Vicolo dell'Osservatorio, 5 00161 Padova, Italy

B. GARILLI: Istituto di Fisica Cosmica, CNR Via Bassini, 15 20133 Milano, Italy

M. MALKAN: Department of Astronomy, University of California, Los Angeles, CA 90024

L. MARASCHI: Università degli Studi di Milano Dipartimento di Fisica Via Celoria, 16 20133 Milano, Italy

G. TAGLIAFERRI: Exosat Observatory, ESTEC Keplerlaan 1, Noordwijk 2200 AG, The Netherlands

E. G. TANZI: Istituto di Fisica Cosmica, CNR Via Bassini, 15 20133 Milano, Italy

A. TREVES: Dipartimento di Fisica Via Celoria, 16 20133 Milano, Italy